RSC Advances

PAPER

View Article Online
View Journal | View Issue

Cite this: *RSC Adv.*, 2022, **12**, 35508

Improving the steric hindrance effect of linear sulfonated acetone–formaldehyde dispersant and its performance in coal–water slurry†

Wenlin Shuai,[abc] Shiwei Wang,[*be] Taotao Sun,[b] Hongfeng Yin,[b] Yu Zu,[b] Gang Yao,[d] Zhonghua Li,[d] Zhaokun Qi[d] and Mei Zhong[*ac]

Dispersants can have a substantial impact on the rheological characteristics of coal–water slurry (CWS). Due to their advantages in cost and synthesis, linear dispersants are currently most often employed in the commercial manufacturing of CWS. However, this kind of dispersant gives limited performance because of its weak adsorption and steric hindrance effect on the coal–water interface. This work describes a new linear dispersant (PSAF) with a significant steric hindrance effect that was created by incorporating phenolic groups into its molecular architecture, which gives higher maximum coal content (63.79 wt%) than that (63.11 wt%) from sulfonated acetone–formaldehyde (SAF). The synthesis mechanism was investigated using GPC, FT-IR and NMR. Various technologies were used to explore the rheological characteristics and dispersion mechanism for CWS prepared with PSAF. PSAF as well as SAF showed monolayer adsorption on the surface of coal and displayed a higher adsorption layer thickness (3.5 nm). PSAF dispersant presents stand-up adsorption rather than lie-down adsorption of SAF because of its strong π–π action, resulting in a stronger steric hindrance effect and improved rheological performance. This work can provide guidelines for the development of a high-performance dispersant as well as an understanding of the dispersal process for CWS.

Received 14th September 2022
Accepted 25th November 2022

DOI: 10.1039/d2ra05802b

rsc.li/rsc-advances

Introduction

Coal is a vital source of carbon-rich fossil energy for China, but its direct combustion poses a serious threat to the environment and human health.[1,2] Coal–water slurry (CWS, which contains around 60–75 wt% coal, 25–40 wt% water, and about 1 wt% dispersant) has been widely used in gasification[3] and is regarded as an attractive alternative to oil as a fuel due to its cleanliness and low cost.[4,5] Highly efficient gasification and combustion necessitate CWS with (i) a high coal content to maximise the heating value and (ii) a low apparent viscosity for pipeline transportation.[6] However, whenever the coal concentration in CWS increases, the particles agglomerate, causing the suspension to settle and lose fluidity and stability. The resulting high viscosity is detrimental to CWS pumping and transportation.[7,8] As a result, the present focus of research is on developing methods for preparing concentrated CWS with increased flowability and stability.[9,10]

It is widely known that a dispersant, in addition to coal particle size distribution and natural coal characteristics (including mineral composition, coal porosity, and surface properties), is an important factor in improving the rheological properties and stability of CWS.[11,12] Many studies have discovered that dispersants can enhance CWS concentration *via* a lowering of coal–water interfacial tension, hydrophilic adjustment of the coal surface, electrostatic force and/or a steric hindrance effect.[13–15] A dispersant has a great influence on the stability of coal–water slurry. The dispersant adsorbed on the surface of coal particles will change the charge density on the surface of coal particles and enhance the electrostatic repulsion among the particles.[7] In addition, the dispersant adsorbed on the particle surface will create steric repulsion and prevent particle adhesion. Electrostatic repulsion and/or steric repulsion are beneficial to improving slurry stability.[16] In general, there is little relationship between electrostatic repulsion and the spatial steric repulsive force of the CWS dispersion system. But in some unique situations, the adsorption behavior of the dispersant will alter due to a change in the double layer

[a]*State Key Laboratory of Chemistry and Utilization of Carbon-Based Energy Resources Jointly Built by Xinjiang Uyghur Autonomous Region and Ministry of Science and Technology, Xinjiang University, Urumqi 830046, Xinjiang, P. R. China. E-mail: zhongmei0504@126.com*

[b]*Ningbo Institute of Materials Technology and Engineering, Chinese Academy of Sciences, Ningbo 315201, Zhejiang, P. R. China. E-mail: wangshiwei@nimte.ac.cn*

[c]*Xinjiang Key Laboratory of Coal Clean Conversion & Chemical Engineering Process, School of Chemical Engineering and Technology, Xinjiang University, Urumqi 830046, Xinjiang, P. R. China*

[d]*Yankuang Xinjiang Coal Chemical Co., Ltd, Urumqi 831408, Xinjiang, P. R. China*

[e]*Zhejiang Institute of Tianjin University, Ningbo, Zhejiang 300192, P. R. China*

† Electronic supplementary information (ESI) available. See DOI: https://doi.org/10.1039/d2ra05802b

structure,[17] which will subsequently lead to a change in the steric repulsive force.

Many dispersants with various structures have been synthesized and evaluated over the last several decades, including one-dimensional (1D) linear (*e.g.*, sulfonated acetone–formaldehyde resin, SAF), two-dimensional (2D) planar (*e.g.*, poly-carboxylic acid, PC), and three-dimensional (3D) spatial dispersants (*e.g.*, tannic acid and acrylic acid copolymer, TTA).[18–20] Although there are many reports on the application of 3D spatial dispersants in coal–water slurry and other slurries, complex processing and high cost hinder their practical industrial application.[21–23] Linear (also known as ribbon) dispersants played an important role in the preparation of CWS, mainly thanks to their low cost and easy synthesis.[24] However, this type of dispersant has poor coal particle adsorption, resulting in performance limitations due to weak interaction between dispersant and coal surface.[25] In addition, the effect of a linear dispersant on improvement in slurry concentration has mainly relied on hydrophilic modification and electrostatic force instead of the steric hindrance effect and reduction in interfacial tension.[19,26,27] In contrast, 2D and 3D dispersants give better dispersion performance due to a superior steric hindrance effect.[27,28] Therefore, improving the coal–water interaction and steric hindrance impact of a linear dispersant by structural design and synthesis is critical.

Recently, Li *et al.* demonstrated that benzene rings in the dispersant could facilitate and strengthen its absorption on the coal surface based on the π–π stacking effect.[29] Based on a similar concept, Zhang *et al.* synthesized an effective dispersant using humic acid as raw material.[30] However, as far as we know, an improvement in the steric hindrance effect for a linear dispersant has not been recorded. A new linear dispersant (PSAF) with a strong steric hindrance effect was synthesized in this study by introducing phenol into its molecular architecture, and the synthesis mechanism was explored. Furthermore, PSAF dispersants were used to prepare highly-concentrated CWS, whose rheological properties were investigated. Finally, the mechanism of coal particle dispersal and stabilization by PSAF dispersant in CWS was investigated, and an adsorption model was proposed. This dispersant is also more environmentally friendly and cost-effective, as phenol can be easily supplied by coal tar creosote from the coal chemical industry.[31] This work can provide guidelines for the development of a high-performance dispersant and an understanding of the dispersal mechanism for CWS.

Experimental

Materials

Formaldehyde solution (37%), acetone, and sodium sulfite were provided by Sinopharm Chemical Reagent Co., Ltd. $HOCH_2SO_3Na$ (97%) and phenol were provided by Maclin Co., Ltd. *o*-Cresol was provided by Aladdin Co., Ltd. 3,5-Dimethylphenol was provided by Tokyo Chemical Industry Co., Ltd. Mixed phenol was prepared by compounding with a mass ratio of 34.76% phenol, 40.82% *o*-cresol, and 24.42% 3,5-dimethylphenol (based on the composition of coal tar creosote). Coal tar creosote was supplied by Juye Runjia Chemical Co., Ltd. Yulin coal samples were kindly donated by Shandong Hualu-Hengsheng Chemical Co., Ltd. Proximate and ultimate analysis data of raw coal samples are shown in Table 1, and their size distribution is shown in Fig. 1.

Table 1 Proximate and ultimate analyses of Yulin coal

Proximate analysis (wt%)				Ultimate analysis[a] (wt%)				
M_{ad}[b]	A_d[c]	V_d[c]	FC_d[c]	C_{daf}	H_{daf}	O_{daf}	N_{daf}	$S_{t,daf}$
6.25	7.10	34.45	58.44	79.91	5.01	13.66	0.99	0.42

[a] Ultimate analysis is on dry ash free basis. [b] M_{ad} refers to the moisture content on air dried basis. [c] A_d, V_d, and FC_d refer to the content of ash, volatile, and fixed carbon on dried basis.

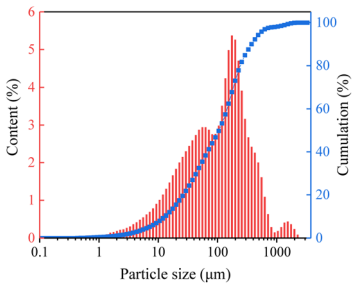

Fig. 1 Particle size distribution of coal sample.

Synthesis of dispersants

PSAF dispersants were synthesized through reactions among sodium sulfite, acetone, phenol, and formaldehyde aqueous solution (37 wt%). The reaction was carried out in a round-bottomed flask equipped with a temperature-controlled electric heating device, a magnetic stirrer, a thermometer, a peristaltic pump, and a reflux condenser. Typically, 8.14 g of sodium sulfite was mixed with 50.00 g of deionized water in a flask by continuous stirring for 10 min, followed by the dropwise addition of 11.40 g of aqueous formaldehyde. After continuous stirring for 5 min, 7.13 g of phenol was added into the above mixture followed by heating at 50 °C for 30 min. Then, a mixture of 12.50 g of acetone and 15.20 g of formaldehyde solution was added dropwise by a peristaltic pump in 20 min. During this process, the reaction solution was heated synchronously to 90 °C. After that, 11.40 g of formaldehyde solution was added into the flask by a peristaltic pump in 10 min followed by continuous stirring for 4–8 h at 90 °C. As a result, a series of PSAF with different molecular weights were obtained, denoted PSAF-*t* according to the reaction time of the final step.

The procedure for synthesizing SAF dispersants was the same as that for PSAF except for the introduction of phenol. Similarly, the SAF dispersant samples were denoted SAF-*t* according to the reaction time of the final step.

The procedure for synthesizing x-PSAF-6 dispersants was the same as that for PSAF-6. The difference is that phenol in the raw materials was replaced by *o*-cresol, 3,5-dimethylphenol, mixed phenol, and coal tar creosote. The x-PSAF-6 dispersant samples

were denoted *o*-PSAF-6, d-PSAF-6, m-PSAF-6, and c-PSAF-6, respectively.

Characterization and measurement

Characterization of dispersants. Solid-state ^{13}C NMR spectra were recorded on a 400 MHz spectrometer (Avance Neo 400M, Bruker, Germany) equipped with a Bruker H-F/X 4 mm CP/MAS probe head at 100.62 MHz for ^{13}C nuclei with TMS as an internal standard. Liquid-state ^{1}H and ^{13}C spectra were collected using a 400 MHz spectrometer (Avance III 400M, Bruker, Germany) employing D_2O or deuterated *N*,*N*-dimethylformamide (DMF-d_7) as the solvent and TMS as the internal standard. The FT-IR spectra were recorded on a spectrophotometer (Nicolet 6700, Thermo Fisher, USA). The molecular weights of the dispersants were measured with a gel permeation chromatograph instrument (Waters 1515, USA). The chromatographic column system consisted of Ultrahydragel 250 and 500 columns in series with pore sizes of 250 and 500 Å, respectively. $NaNO_3$ solution (0.1 g L^{-1}) was used as mobile phase flowing (1 mL min^{-1}) at a temperature of 35 °C.[32]

Apparent viscosity and static stability of CWS. The coal particles were gradually mixed in a beaker filled with dispersant solutions with a concentration of 0.2 weight percent (based on the quantity of dry coal).[35] To ensure that the CWS was homogenous, the mixture was continuously agitated at 800 rpm for 3 minutes. The apparent viscosity of CWS was measured using a rheometer (NXS-4CP, Chengdu Instrument Plant, China), under the conditions of a temperature of 20 °C and a shear rate of 100 s^{-1}. A water separating test (water separating ratio, wt%) and the storage period (h) were used to assess the stability of CWS.[33] In detail, fresh slurry was stored in a glass cylinder (CWS layer 100 mL in volume) at room temperature for 24 h. Then, the amount of water extracted from the CWS was measured. The water separating ratio W_s was calculated according to eqn (1):

$$W_s = m_w/m_c \times 100\% \quad (1)$$

m_w (g) refers to the mass of upper water in the CWS after 24 hours, and m_c (g) is the total mass of CWS.

Zeta potential measurements. A zetasizer (Nano ZS, Malvern, UK) was used to assess the zeta potential of the coal particles in CWS.[34] 1 g of coal particles was suspended in 25 mL of water or dispersant-containing solution (1000 mg L^{-1}). This dilute CWS was shaken for 12 hours at room temperature to achieve adsorption equilibrium before centrifugal sedimentation at 8000 rpm for 10 minutes. Then, the upper clear solution from the CWS was extracted for the zeta potential test.

Adsorption measurements. The amount of dispersant adsorbed on coal particles was calculated by determining the amount of free water in the transparent layer. In detail, a series of 25 mL dispersant solutions with concentrations of 0, 100, 200, 300, 500, 600, 800, 1000, and 1200 mg L^{-1} were prepared. Then, 1 g of coal sample was added to the above dispersant solutions and shaken for 12 hours before centrifugal sedimentation at 8000 rpm for 10 minutes. The mass concentration of dispersant was determined with a UV spectrophotometer (Lambda 950, PerkinElmer, USA) based on the calibration curve (Fig. S1†). The details of the calculation are shown in ref. 35.

Measurements of thickness of dispersant adsorption layer. The thickness of the dispersant adsorption layer was tested by X-ray photoelectron spectroscopy (Shimadzu, UK, Al Kα, $h\nu$ = 1486.6 eV). Si in coal was selected as the characteristic element to calculate the adsorption layer thickness of the dispersant on coal. The photoelectron intensity of Si_{2p} will decay after it travels through the dispersant adsorption layer. Then, the change in photoelectron intensity will be used to evaluate the thickness of the dispersant adsorption layer. 1 g of coal particles were suspended in 25 mL of water or dispersant-containing solution (1000 mg L^{-1}). This dilute CWS was shaken for 12 hours at room temperature to achieve adsorption equilibrium before centrifugal sedimentation at 8000 rpm for 10 minutes. The sublayer was precipitated and dried under vacuum at 40 °C to obtain a dry solid powder. The details of the calculation are shown in ref. 33.

Low-field NMR. The existing state of water in CWS was characterized using MesoMR23-040V NMR (Suzhou Niumag Analytical Instrument Corp., China) at 23 MHz. Different states of water show different transverse relaxation times (T_2) in NMR signals. The area of the signal peak is proportional to the water content. The preparation process of the samples is the same as that described in Apparent viscosity and static stability of CWS.

Contact angle measurements. Contact angles between the water and coal or coal-adsorbed dispersants were measured on a DCAT21 dynamic contact angle analyser (Dataphysics, Germany). 5 g of coal particles (Yulin coal) were suspended in 125 mL of water or dispersant-containing solution (1000 mg L^{-1}). This dilute CWS was shaken for 12 hours at room temperature to achieve adsorption equilibrium before centrifugal sedimentation at 8000 rpm for 10 minutes. The sublayer was precipitated and dried under vacuum at 40 °C to obtain a dry solid powder. The coal powder was pressed into round tablets under the same pressure for measurement, and then a drop of deionized water was dripped onto the tablets. Then, photographs of the coal–water interfaces were obtained using a digital camera in the goniometer.

Results and discussion

Characterization of dispersants

A series of PSAF-*t* and SAF-*t* dispersants were synthesized by the steps described in Synthesis of dispersants. The molecular weight distribution of these synthetic dispersants was analyzed by gel permeation chromatography (GPC) and the results are shown in Fig. 2a and Table S1.† As shown in Fig. 2a, the dispersants contain some unreacted monomers or prepolymers. In general, the molecular weight of the SAF-*t* and PSAF-*t* dispersants gradually increased with an extension of reaction time. As shown in Table S1,† the molecular weights of SAF-*t* dispersants (*ca.* 50 000–65 000 Da) are obviously higher than those of PSAF-*t* dispersants (*ca.* 6500–12 000 Da). The polydispersity indexes of PSAF-*t* (*ca.* 1–2) are lower than those of SAF-*t* (*ca.* 3–5), indicating that their molecular weight distribution is narrower. The typical PSAF-6 and SAF-4 samples were

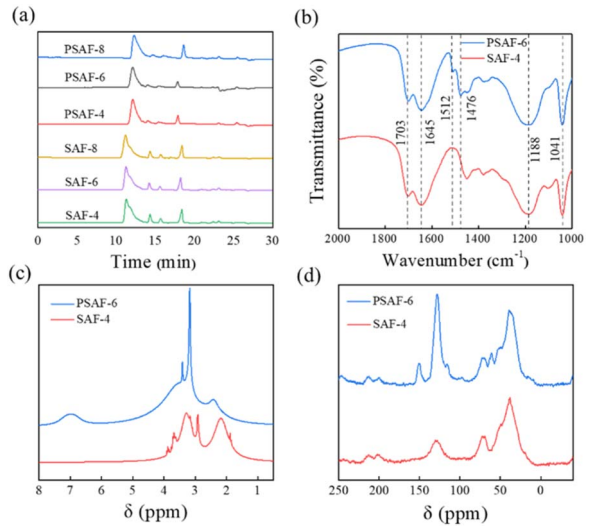

Fig. 2 (a) GPC analysis for PSAF-*t* and SAF-*t*. (b) FT-IR spectra of PSAF-6 and SAF-4. (c) ^{1}H NMR (D_2O) and (d) ^{13}C CP/MAS NMR spectra of PSAF-6 and SAF-4.

selected for further structural characterization analysis. To avoid the effect of unreacted precursors in the product on structural analysis, the samples need to be purified. The specific treatment process was as follows: the as-synthesized PSAF-6 and SAF-4 samples were dialyzed (molecular weight cutoff for 3500 Da) for 5 and 3 days, respectively. Subsequently, the purified samples were freeze-dried to obtain powdered products for further characterization and analysis. GPC was used to detect the molecular weight distributions of PSAF-6 and SAF-4 and to evaluate the degree of purification (Fig. S2†). Infrared spectra of PSAF-6 and SAF-4 dispersants are shown in Fig. S3† (full spectra) and Fig. 2b (partial spectra). PSAF-6 and SAF-4 dispersants contained O–H (3449 cm^{-1}), C–H (2928 and 2869 cm^{-1}), C=O (1703 cm^{-1}), C=C (1645 cm^{-1}), S=O (1188 cm^{-1}) and S–O (1041 cm^{-1}), and C–S (768 and 610 cm^{-1}). Unlike SAF-4, the PSAF-6 dispersant has benzene ring skeleton vibration absorption peaks (1512 and 1476 cm^{-1}), indicating the effective introduction of phenol structural units into the aliphatic molecular chain.[36,37] Fig. 2a and d show ^{1}H NMR and ^{13}C CP/MAS NMR spectra of PSAF-6 and SAF-4. According to ^{1}H NMR spectra, proton peaks of $-CH_2-C-$ (δ = 1.00–2.68 ppm), $-CH_2-S-$ (δ= 2.70–3.02 ppm), $-CH_2-O-$ (δ= 3.02–4.40 ppm), –OH (δ = 4.60–6.01 ppm) and CH_2=C– (δ = 4.60–6.01 ppm) are found in both PSAF-6 and SAF-4. Differently, PSAF-6 dispersant contains proton peaks of benzene ring (δ = 6.4–8 ppm). According to ^{13}C CP/MAS NMR spectra, the dispersants of PSAF-6 and SAF-4 contain or $-CH_2-$ (δ = 0–61.16 ppm), $-CH_2-O-$ (δ = 63.56–84.19 ppm), –C=C– (δ = 110.01–147.05 ppm) and –C=O (δ= 191.12–223.36 ppm). Differently, chemical shifts of aromatic ring carbon (δ = 108.81–155.83 ppm) were observed in PSAF-6, indicating that the phenol structural units have been successfully introduced into the aliphatic molecular chain. This is consistent with the results of infrared spectroscopy. However, it is difficult to reveal reaction mechanism and chemical structure of PSAF dispersant based on FT-IR and NMR spectra.

Investigation on synthesis mechanism

The mechanism and chemical structure of this aliphatic dispersant have been studied extensively, but it is still difficult to understand them clearly because of its complexity.[38] The hydrolysis of sodium sulfite to generate sodium bisulfite, which reacts with formaldehyde to generate $HOCH_2SO_3Na$, were widely considered to be the initial reactions of the aliphatic dispersant.[39–41] To understand the substitution position of $HOCH_2SO_3Na$ on the molecular chain of PSAF, the reaction (Fig. 3a) of $HOCH_2SO_3Na$ with acetone was performed and the product was analyzed by NMR. As shown in Fig. 3b, peaks at 3.76 ppm could be ascribed to the chemical shift of the protons in $-C-CH_2-SO_3Na$, while the peak at 2.14 ppm could be assigned to the chemical shift of the protons in CH_3-C=O and $-C-CH_2-C$=O. These results indicated that the carbon atom of $HOCH_2SO_3Na$ is easily linked to the α-C atom of acetone under catalysis by OH^-. In addition, the peak at 4.36 ppm is caused by the proton of the unreacted $HOCH_2SO_3Na$ (Fig. S4†). Fig. 3c represents ^{13}C NMR spectra for the reaction product of $HOCH_2SO_3Na$ and acetone. Peaks between 43.60 and 63.67 ppm

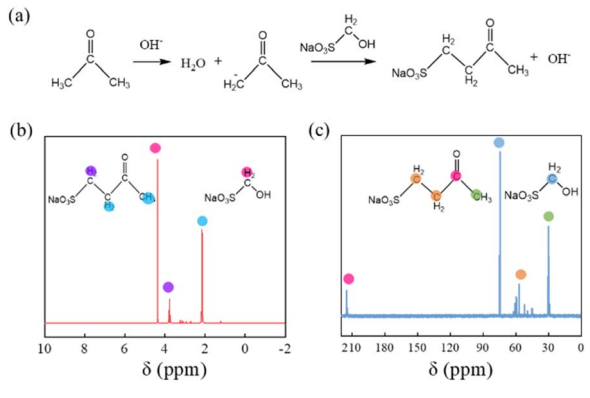

Fig. 3 (a) Dehydration reaction of $HOCH_2SO_3Na$ and acetone in alkaline aqueous solution. (b) ^{1}H NMR and (c) ^{13}C NMR spectra for the product of $HOCH_2SO_3Na$ and acetone (D_2O).

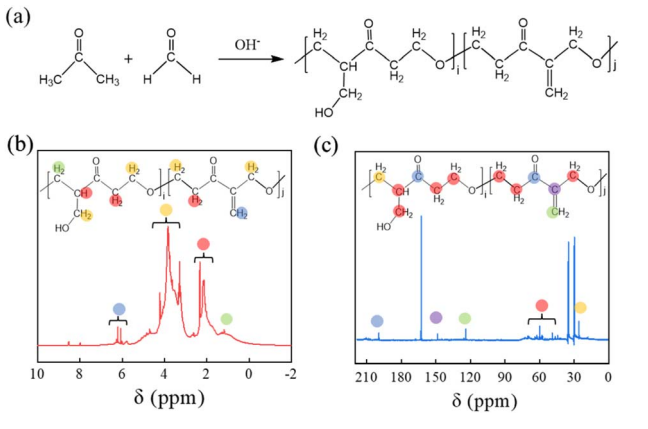

Fig. 4 (a) Reaction of formaldehyde and acetone in alkaline aqueous solution. (b) ^{1}H NMR and (c) ^{13}C NMR spectra for the product of formaldehyde and acetone (DMF-d_7).

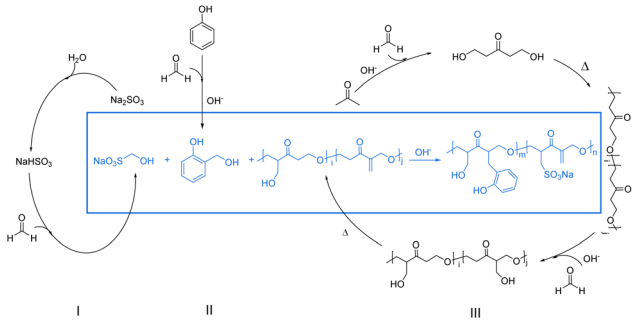

Fig. 5 Plausible synthesis mechanism of the PSAF dispersant.

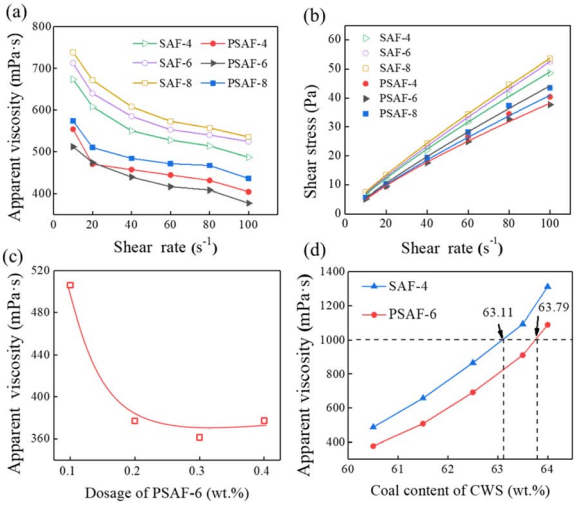

Fig. 6 (a) Effect of the shear rate on the apparent viscosity of CWS. (b) Effect of shear rate on the shear stress of CWS. (c) Effect of dosage of PSAF-6 dispersant on the apparent viscosity of CWS. (d) Effect of the coal content on the apparent viscosity of CWS.

could be ascribed to chemical shifts of carbon atoms in $-CH_2-$, while those at 214.72 and 30.18 ppm could be attributed to chemical shifts of carbon atoms in –C=O and $-CH_3$, respectively. These results further support the conclusions from ^{1}H NMR spectroscopy. In addition, the peak at 74.53 ppm is designated as the carbon atom of unreacted $HOCH_2SO_3Na$.

The polymerization of formaldehyde and acetone was performed and the products were analyzed by GPC, FT-IR, and NMR to understand the formation of major molecular chains in detail (Fig. 4a). As shown in Fig. S5,† the reaction product has an M_W of 2723 Da, which indicates that formaldehyde and acetone could be polymerized under catalysis by OH^-. Fig. S6† presents infrared characteristic peaks of the polymerization product. The peaks at 2930 cm^{-1} and 2868 cm^{-1} result from the stretching vibration of C–H, whose bending vibrations appear at 1452 cm^{-1} and 1379 cm^{-1}. The characteristic peak of O–H appears at 3435 cm^{-1}, while the peaks at 1702 cm^{-1} and 1095 cm^{-1} can be assigned to the stretching vibrations of C=O and C–O, respectively. Significantly, the characteristic peak of C=C appears at 1661 cm^{-1}, indicating that this polymer contains C=C groups. ^{1}H and ^{13}C NMR analysis were further carried out to verify the chemical structure of this product. As shown in Fig. 4b, peaks from 3.12 to 4.43 ppm could be assigned to proton chemical shifts of $-C-CH_2-O-$. It is worth noting that peaks from 1.58 to 2.94 ppm and from 6.07 to 6.22 ppm are attributed to proton chemical shifts of $-C-CH_2-C{=}O$ and $CH_2{=}C-$, respectively. The peaks from 1 to 1.58 ppm could be ascribed to proton chemical shifts of $-C-CH_2-C-$. As shown in the ^{13}C NMR spectrum (Fig. 4c), characteristic carbon peaks of DMF-d_7 solvent were observed (162.57, 35.03, and 29.88 ppm). The peak at 199.38 ppm is caused by the carbon atom in –C=O, while those at 148.59 and 124.03 ppm correspond to carbons atom in –C=C–. The peaks from 40.03 to 65.01 ppm are ascribed to carbon atoms in $-CH_2-O-$, –CH–C–, and $-CH_2-C-$ (linked to the carbonyl group), and the peaks at 25.89 ppm are ascribed to carbon atoms in $-CH_2-C-$. These results correspond perfectly with the ^{1}H NMR analysis.

Based on the above analysis, a possible synthesis mechanism of the PSAF dispersant is proposed (Fig. 5). As described in Synthesis of dispersants, the synthesis of PSAF dispersant includes three main stages. Two reactions occur in the first stage: the addition of formaldehyde to sodium bisulfite derived from sodium sulfite to generate $HOCH_2SO_3Na$ (i) and the addition reaction of formaldehyde with phenol (ii).[42] In the second stage, formaldehyde and acetone begin to polymerize based on aldol condensation and a Michael addition reaction mechanism (iii).[43,44] In the final stage, the addition product of phenol and sodium bisulfite reacts with the α-C in a prepolymer of formaldehyde and acetone[42] to generate a new C–C bond. At the same time, this prepolymer will further polymerize with formaldehyde and acetone to form the final dispersant.

Rheological behavior of CWS

The viscosity-reducing capacities of PSAF-*t* dispersants compared to those of conventional SAF-*t* dispersants were evaluated. The relationship between the apparent viscosity and shear rate of CWS with 60.5 wt% solid content and 0.2 wt% dispersants of coal is shown in Fig. 6a. The CWS behaves as a non-Newtonian fluid with shear thinning. Apparently, PSAF-*t* dispersants have a better viscosity reduction effect than SAF-*t* dispersants and the apparent viscosity increases in the order PSAF-6 < PSAF-4 < PSAF-8 < SAF-4 < SAF-6 < SAF-8 at a shear rate of 100 s^{-1}. The rheological data for CWS were fitted by the Herschel–Bulkley model ($\tau = \tau_y + K \times r^n$), in which τ, τ_y, K, r, and n represent the shear stress (Pa), yield stress (Pa), consistency coefficient (Pa s^n), shear rate (s^{-1}), and rheological index, respectively.

As shown in Fig. 6b, the shear stress increased linearly with increasing shear rate for all the slurries, and the rheological index, n, was less than 1, indicating again the non-Newtonian pseudoplastic behaviors of CWS (Table S2†). Moreover, the τ_y of CWS with PSAF-6 (−1.62 Pa) was lower than all the others.[45,46] The smaller yield stress indicated higher redispersion ability.[28] Fig. 6c gives the effect of dosage for the best PSAF-6 dispersant on the apparent viscosity of CWS which was investigated with 60.5 wt% solid content at a shear rate of 100 s^{-1}. The apparent viscosity of CWS decreases from 506 mPa s (0.1 wt%) to 377 mPa s (0.2 wt%); then, it is stable with an increase in dosage of

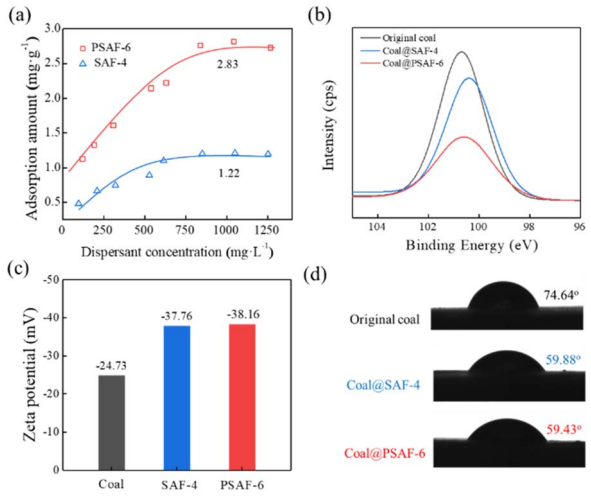

Fig. 7 (a) Adsorption isotherms of SAF-4 and PSAF-6 dispersants on the surface of coal particles. (b) Si_{2p} scanning spectra of original coal, coal@SAF-4, and coal@PSAF-6. (c) Zeta potentials of coal with and without adsorbed SAF-4 and PSAF-6 dispersants (1000 mg L^{-1}). (d) Contact angles of distilled water on original coal, coal@SAF-4, and coal@PSAF-6 surface. (The mass concentration of the dispersant solutions is 1000 mg L^{-1}.)

dispersant. At low dosage, the dispersant on the surface of coal particles does not reach adsorption saturation, so it shows a limited viscosity reduction effect.[47] The adsorption on the coal surface reached saturation when the dosage was raised to 0.2 wt%; then, the viscosity reduction effect underwent almost no enhancement with a further increase in the dosage. Fig. 6d shows the effect of slurry concentration on the apparent viscosity of CWS with PSAF-6 and SAF-4 dispersants with 0.2 wt% dispersants of coal at a shear rate of 100 s^{-1}. The apparent viscosity of CWS increases as the coal concentration increases and the corresponding coal concentrations reached 63.79 wt% (PSAF-6) and 63.11 wt% (SAF-4) under an apparent viscosity of 1000 mPa s, respectively.

Adsorption investigation of dispersants on the coal surface

To understand the mechanism of better dispersion performance of PSAF compared with SAF dispersants, their adsorption behavior, electrostatic repulsion and wettability on the coal surface were investigated. Fig. 7a depicts the adsorption capacity of dispersants on the coal surface *vs.* equilibrium dispersant concentration at 20 °C. This phenomenon showed that the adsorption quantity increased considerably with the increase in dispersant concentration at the beginning and then attained a plateau. The adsorption curves were fitted by the Langmuir adsorption and Freundlich adsorption models, and the fitting results are shown in Table S3.† The correlation coefficients (R^2) of the Langmuir equation (0.981) for the dispersants were both larger than those of the Freundlich equation (0.967 or 0.978). This shows that the Langmuir adsorption model can properly describe the adsorption of dispersant on the surface of coal particles and shows the characteristics of monolayer adsorption. The saturated adsorption capacity of SAF-4 on the coal surface is 1.47 mg g^{-1}, lower than that of PSAF-6 on the coal surface of 3.50 mg g^{-1}. X-ray photoelectron spectroscopy (XPS) was used to evaluate the adsorption layer thickness of dispersants on the coal surface. Si was selected as the characteristic element because of its existence in coal but not in the dispersants. The XPS spectra and Si_{2p} spectra of coal particles with and without dispersants are shown in Fig. S7 and 7b,† respectively. The adsorption layer thickness can be appraised through the attenuation value of an Si_{2p} photoelectron passing through the dispersant adsorption layer. The result in Table S4† indicated larger adsorption layer thickness for PSAF-6 (3.5 nm) than SAF-4 (0.9 nm), which is consistent with the results of the adsorption capacity, indicating that the steric effect of PSAF-6 adsorbed on the surface of coal particles is stronger.

According to the DLVO theory, electrostatic repulsion is significant in the dispersion and stabilization of CWS.[48] As shown in Fig. 7c, zeta potentials of coal particles in CWS without a dispersant was approximately −24.73 mV. This indicated that the surface coal particles were negatively charged due to the existence of oxygenic groups, which would be ionized in aqueous environments.[49,50] As expected, the zeta potentials of coal particles shifted to more negative values in the presence of PSAF-6 and SAF-4 (−38.16 and −37.76 mV) because of the dispersant absorption on coal particles.[28] However, although the adsorption capacities of PSAF-6 and SAF-4 on the surface of coal particles are different, they give comparable zeta potential and electrostatic repulsion. Previous studies have shown that the wettability of a dispersant on the surface of coal particles is a key factor affecting the concentration of coal–water slurry.[51] The contact angles of water on coal or coal-adsorbed dispersant surfaces were measured to indicate the changes in surface hydrophobicity or hydrophilicity. As shown in Fig. 7d, the contact angles of coal, coal@SAF-4, and coal@PSAF-6 were 74.64°, 59.88°, and 59.43°, respectively. This result indicates that SAF-4 and PSAF-6 present comparable wettability of the coal surface. This phenomenon can be explained by their similar chemical functional groups and hydrophilicity.

Dispersive mechanism

Low-field nuclear magnetic resonance technology was used to analyze the water status in CWS, which helps to explain the rheological properties according to a microscopic mechanism.

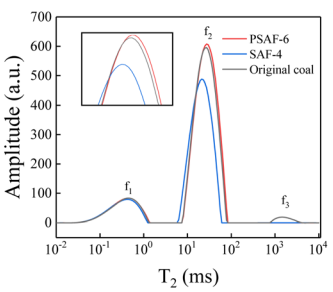

Fig. 8 T_2 spectra of CWS prepared without a dispersant and with SAF-4 and PSAF-6 dispersants.

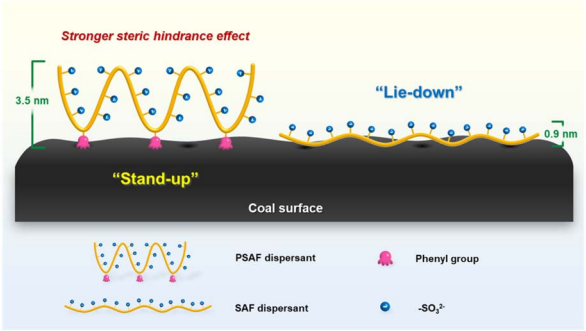

Fig. 9 Illustration of the internal structure of CWS prepared with PSAF and SAF dispersants.

T_2 reflects the chemical environment of the proton in the sample, which is related to the binding force of the proton and its degree of freedom. Thus, T_2 becomes shorter with an increase in the binding degree of the proton or a decrease in the degrees of freedom.[52,53] As shown in Fig. 8, there are three water states in CWS: T_2 = 0.01–2 ms representing adsorbed water, T_2 = 5–100 ms representing interstitial water, and T_2 = 500–5000 ms representing free water. The areas of the peaks are a measure of the amount of water in different states and results are shown in Table S5.† The free water content of CWS prepared with dispersants is obviously lower than that of CWS prepared without a dispersant. From this phenomenon it is revealed that the dispersant improves the hydrophilicity of the coal surface, and the free water is adsorbed by the composite particles (coal particle adsorbed dispersant), which is transformed into adsorbed or interstitial water.[54] Compared with CWS prepared with SAF-4 dispersant, the adsorbed water content of CWS prepared with PSAF-6 is lower and the interstitial water is higher. This phenomenon may be caused by the stronger adsorption of PSAF-6 on the coal surface, which blocks the channel from interstitial water to adsorbed water.[54,55]

Given the structural characteristics and the above experimental results for PSAF dispersants during CWS preparation, the possible interactions between coal particles, dispersants, and water can be inferred. Fig. 9 shows a schematic of the internal structure for CWS prepared with PSAF dispersants, which is significantly different from that of SAF dispersants. PSAF dispersants displayed similar wettability and electronegativity to SAF, which was verified by research on contact angle and zeta potential experiments. The difference is that the adsorption capacity and thickness of PSAF on the coal surface are significantly greater than that of SAF, leading to a stronger steric hindrance effect. From a microscopic perspective, aromatic rings and aliphatic groups in the molecular chain of the PSAF dispersant compete for adsorption, interacting with the aromatic hydrophobic regions and hydrophilic sites (carboxyl, hydroxyl, amino, *etc.*) of the coal surface. The PSAF dispersant undergoes stand-up adsorption rather than the horizontal adsorption of SAF due to strong π–π action. This stand-up adsorption behavior leads to a change in water status and a steric hindrance effect, seriously affecting the CWS performance.

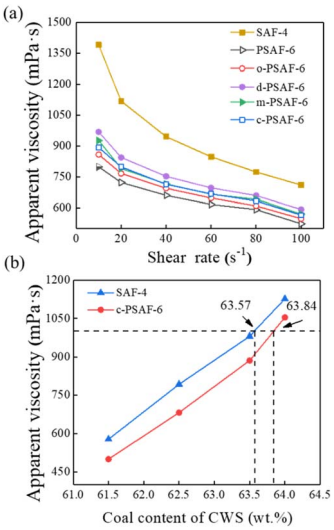

Fig. 10 (a) Effect of shear rate on the apparent viscosity of CWS. (b) The effect of coal content on the apparent viscosity of CWS.

Synthesis of x-PSAF-6 dispersants and their dispersive performance

Given that coal tar creosote is a cost-effective phenol source, *o*-cresol, 3,5-dimethylphenol, mixed phenol, and coal tar creosote were used to replace phenol to synthesize a series of x-PSAF-6 dispersants. As shown in Table S6 and Fig. S8,† x-PSAF-6 dispersants show similar molecular weight (*ca.* 12 000–17 000 Da) to PSAF-6 but lower than that of SAF-4. Fig. 10a shows the apparent viscosity *vs.* shear rate of CWS with 0.2 wt% dispersant (based on coal weight) and 60.5 wt% coal particles. The apparent viscosity of CWS with x-PSAF-6 and SAF-4 dispersants decreased dramatically and then gently with an increase in shear rate (shear thinning behavior), which indicated that CWS prepared by these dispersants were pseudoplastic fluids. Notably, the x-PSAF-6 dispersants give a better viscosity reduction effect than that of the SAF-4 dispersant at a shear rate of 100 s^{-1}. Fig. 10b gives the relationship between the apparent viscosity of CWS and the solid concentration. The maximum slurry concentration was the concentration at which the apparent viscosity of the CWS reached 1000 mPa s. The maximum slurry concentration of CWS prepared with c-PSAF-6 (63.84 wt%) was, as expected, higher than that of SAF-4 dispersant (63.57 wt%). These results show that the cost of PSAF dispersants can be reduced by using cheaper coal tar creosote instead of phenol. Additionally, a comparison of CWS water separating ratio prepared from x-PSAF-6 and SAF-4 dispersants within 24 h is shown in Fig. S9.† In general, the CWS prepared from x-PSAF-6 dispersants show lower water separating ratio than that from SAF-4 for Yulin coal.

Conclusions

Dispersants can greatly enhance the rheological characteristics and stability of CWS. Typically, linear dispersants play an important role in the preparation of CWS due to their low cost

and easy synthesis. However, due to the lack of steric hindrance action, this type of dispersant performs insufficiently well. In this study, phenolic groups were added to the aliphatic main chain to create a novel linear dispersant (PSAF) with a high steric hindrance effect. The structure, synthesis mechanism, rheological behaviors, and dispersing mechanism of PSAF dispersants for CWS were investigated using various technologies. The PSAF dispersant undergoes stand-up adsorption instead of lie-down adsorption, which leads to a stronger steric hindrance effect and better rheological performance. This dispersant can also be prepared using coal tar creosote as the phenol, giving it good industrial application prospects. This work can provide guidelines for a high-performance dispersant for CWS.

Author contributions

Wenlin Shuai: investigation, methodology, data curation, writing-review & editing; Shiwei Wang: investigation, methodology, writing-original draft, writing-review & editing, supervision; Taotao Sun: data curation, software; Hongfeng Yin: supervision, project administration; Yu Zu: conceptualization, project administration, funding acquisition; Gang Yao: resources, validation; Zhonghua Li: resources, validation; Zhaokun Qi: resources, validation; Mei Zhong: supervision, writing-review & editing, funding acquisition.

Conflicts of interest

There are no conflicts to declare.

Acknowledgements

This work is partly supported by the National Science Foundation of China (Grant No. 22072171 and 21902169), Outstanding Youth Fund of Xinjiang Uygur Autonomous Region (Grant No. 2020Q001), and the Postdoctoral Science Preferential Funding of Zhejiang Province, China (Grant No. ZJ2020005).

References

1 Q. Yi, W. Li, J. Feng and K. Xie, *Chem. Soc. Rev.*, 2015, **44**, 5409.
2 Y. Shen, X. Liu, T. Sun and J. Jia, *RSC Adv.*, 2012, **2**, 8867.
3 S. Hu, L. Liu, X. Yang, J. Li, B. Zhou, C. Wu, L. Weng and K. Liu, *RSC Adv.*, 2019, **9**, 32911.
4 E. Xu, S. Chen, Y. Dong, Z. Miao, X. Jiang, L. Cui, X. Meng and G. Wu, *Fuel*, 2021, **292**, 120394.
5 Z. Meng, Z. Yang, Z. Yin, Y. Li, X. Song, J. Zhao and W. Wu, *Powder Technol.*, 2020, **359**, 261.
6 D. Yao, H. Zhao, Z. Chen and H. Liu, *Fuel*, 2022, **317**, 123461.
7 Y. Zhang, S. Hu, X. Yang, F. Jiang, C. Wu, J. Li and K. Liu, *Colloids Surf., A*, 2021, **630**, 127544.
8 S. K. Mishra, P. K. Senapati and D. Panda, *Energy Sources*, 2010, **24**, 159.
9 D. Yang, X. Qiu, M. Zhou and H. Lou, *Energy Convers. Manage.*, 2007, **48**, 2433.
10 X. Qiu, M. Zhou, D. Yang, H. Lou, X. Ouyang and Y. Pang, *Fuel*, 2007, **86**, 1439.
11 F. Boylu, H. Dinçer and G. Ateşok, *Fuel Process. Technol.*, 2004, **85**, 241.
12 W. Yuchi, B. Li, W. Li and H. Chen, *Coal Prep.*, 2005, **25**, 239.
13 G. Zhang, J. Li, J. Zhu, Q. Qu and W. Xiong, *Powder Technol.*, 2014, **254**, 572.
14 J.-H. Park, Y.-J. Lee, M.-H. Jin, S.-J. Park, D.-W. Lee, J.-S. Bae, J.-G. Kim, K. H. Song and Y.-C. Choi, *Fuel*, 2017, **203**, 607.
15 P. Liu, M. Zhu, Z. Zhang, Y.-K. Leong, Y. Zhang and D. Zhang, *Fuel Process. Technol.*, 2017, **156**, 27.
16 D. Das, S. K. Das, P. K. Parhi, A. K. Dan, S. Mishra and P. K. Misra, *Energy Nexus*, 2021, **4**, 100025.
17 U. Behera, S. K. Das, D. P. Mishra, P. K. Parhi and D. Das, *ACS Omega*, 2021, **6**, 22820–22830.
18 R. Xu, W. Zhuang, Q. He, J. Cai, B. Hu and J. Shen, *AIChE J.*, 2009, **55**, 2461.
19 M. Zhou, X. Qiu, D. Yang and X. Ouyang, *J. Dispersion Sci. Technol.*, 2009, **30**, 353.
20 K. Zhang, X. Zhang, L. e. Jin, Q. Cao and P. Li, *Fuel*, 2017, **200**, 458.
21 A. Kumar Dan, B. Biswal, M. Das, S. Parida, P. Kumar Parhi and D. Das, *J. Mol. Liq.*, 2022, **360**, 119547.
22 S. K. Das, A. K. Dan, U. Behera, A. K. Tripathi, M. Behari, D. Das and P. K. Parhi, *Case Stud. Chem. Environ. Eng.*, 2021, **4**, 100156.
23 M. Behari, A. M. Mohanty and D. Das, *Powder Technol.*, 2022, **407**, 117620.
24 S. Hu, F. Jiang, J. Li, C. Wu, K. Liu and Y. Chen, *Colloids Surf., A*, 2021, **628**, 127245.
25 L. Li, L. Zhao, Y. Wang, J. Wu, G. Meng, Z. Liu, J. Zhang, B. Hu, Q. He and X. Guo, *Energy Fuels*, 2018, **32**, 8310.
26 S. Hu, Y. Chen, C. Wu, J. Li and K. Liu, *Colloids Surf., A*, 2020, **606**, 125450.
27 X. Meng, T. Zhang, G. Wu, R. Chu, L. Fan, X. Jiang, Y. Li, W. Zhang, Y. Wan, W. Li and X. Li, *Colloids Surf., A*, 2022, **643**, 128812.
28 K. Zhang, J. Ma, B. Lyu, G. Shi, B. Zhou and Y. Tian, *Fuel*, 2020, **274**, 117860.
29 L. Li, C. Ma, S. Hu, M. He, H. Yu, Q. Wang, X. Cao and X. You, *Int. J. Min. Sci. Technol.*, 2021, **31**, 515.
30 W. Zhang, J. Luo, Y. Huang, C. Zhang, L. Du, J. Guo, J. Wu, X. Zhang, J. Zhu and G. Zhang, *Fuel*, 2020, **262**, 116576.
31 T. Zhu, J. Dong, L. Niu, G. Chen, L. Ricardez-Sandoval, X. Wen and G. Bai, *Appl. Clay Sci.*, 2021, **203**, 106003.
32 C. Chen, D. Jin, X. Ouyang, L. Zhao, X. Qiu and F. Wang, *Fuel*, 2018, **223**, 366.
33 J. Zhu, P. Wang, Y. Li, J. Li and G. Zhang, *Fuel*, 2017, **190**, 221.
34 H. Bouhamed, A. Magnin and S. Boufi, *J. Colloid Interface Sci.*, 2006, **298**, 238.
35 R. Li, D. Yang, H. Lou, M. Zhou and X. Qiu, *Energy Convers. Manage.*, 2012, **64**, 139.
36 Z. Pu, X. Fan, J. Su, M. Zhu and Z. Jiang, *Colloid Polym. Sci.*, 2022, **300**, 167.
37 N. Hong, Y. Li, W. Zeng, M. Zhang, X. Peng and X. Qiu, *RSC Adv.*, 2015, **5**, 21588.

38 H. D. Yan, Y. F. Wang and Z. L. Quan, *Adv. Mater. Res.*, 2012, **554–556**, 878.
39 L. M. Carvalho and G. Schwedt, *J. Chromatogr. A*, 2005, **1099**, 185.
40 V. Ramdugwar, H. Fernandes and P. Gadekar, *Int. J. Adhes. Adhes.*, 2022, **115**, 103122.
41 N. A. Costa, J. Pereira, J. Ferra, P. Cruz, J. Martins, F. D. Magalhães, A. Mendes and L. H. Carvalho, *Wood Sci. Technol.*, 2013, **47**, 1261.
42 C. Liu, H. Cao, S. Jin, Y. Bao, Q. Cheng and Z. Rao, *Sol. Energy Mater. Sol. Cells*, 2022, **243**, 111789.
43 A. Axelsson, E. Hammarvid, M. Rahm and H. Sundén, *Eur. J. Org. Chem.*, 2020, 5436.
44 M. Ai, *J. Catal.*, 1987, **106**, 273.
45 C. Qian, L. Zhao, X. Ge and X. Chen, *Chin. J. Chem. Eng.*, 2020, **28**, 566.
46 J. Huang, J. Xu, D. Wang, L. Li and X. Guo, *Ind. Eng. Chem. Res.*, 2013, **52**, 8427.
47 L. Du, G. Zhang, D. Yang, J. Luo, Y. Liu, W. Zhang, C. Zhang, J. Li and J. Zhu, *R. Soc. Open Sci.*, 2021, **8**, 201480.
48 K. Zhang, Y. Hou, Z. Ye, T. Wang, X. Zhang and C. Wang, *Fuel*, 2022, **318**, 123608.
49 M. K. R. Konduri and P. Fatehi, *Fuel Process. Technol.*, 2018, **176**, 267.
50 Y. Qin, D. Yang, W. Guo and X. Qiu, *J. Ind. Eng. Chem.*, 2015, **27**, 192.
51 X. Jiang, S. Chen, L. Cui, E. Xu, H. Chen, X. Meng and G. Wu, *J. Cleaner Prod.*, 2022, **330**, 129881.
52 C. Wang, H. Zhao, Z. Dai, W. Li and H. Liu, *Fuel*, 2019, **235**, 639.
53 J. Zhang, H. Zhao, C. Wang, W. Li, J. Xu and H. Liu, *Fuel*, 2016, **177**, 19.
54 J. Liu, R. Wang, Y. Hu, J. Zhou and K. Cen, *Energy Fuels*, 2013, **27**, 2883.
55 S. Hu, F. Jiang, B. Zhao, Y. Chen, C. Wu, J. Li and K. Liu, *Energy Fuels*, 2021, **35**, 2006.